scientific reports

OPEN

Study on isothermal crystallization kinetics of $Zr_{55.7}Cu_{22.4}Ni_{7.2}Al_{14.7}$ bulk amorphous alloy

Weijian Zhang[1], Pingjun Tao[1✉], Yugan Chen[1], Junfeng Si[2], Zhenghua Huang[3], Kunsen Zhu[1] & Yuanzheng Yang[1]

$Zr_{55.7}Cu_{22.4}Ni_{7.2}Al_{14.7}$ alloy bars were prepared by copper mold suction casting, and the structure and thermodynamic properties of the prepared specimens were characterized by X-ray diffractometer and differential scanning calorimeter. Furthermore, isothermal crystallization mechanism and crystallization activation energy were investigated by Johnson–Mehl–Avrami model and Arrhenius equation. The results show that the structure of the specimen is amorphous. The glass transition temperature (T_g), onset crystallization temperature (T_x) and crystallization peak temperature (T_p) are 713 K, 779 K, and 781 K, respectively, and supercooled liquid region ($\Delta T = T_x - T_g$) is 66 K. The crystallization incubation times are shortened and the crystallization transformation rates increase with temperature rising. As the crystallization volume fraction increases, the crystallization nucleation rate shows a trend of first increasing and subsequently decreasing, while the activation energy decreases monotonously, in the same time, the crystallization behavior transforms from interface-controlled to diffusion-controlled growth. The thermal stability of amorphous alloy is also discussed.

Amorphous alloys are new amorphous metallic glass materials with excellent mechanical, physical and chemical properties of both general metals and glass, made by modern rapid solidification metallurgical techniques. Amorphous alloys, also known as metallic glasses or liquid metals, are composed of a short-range ordered, long-range disordered glassy structure with a more uniform structure and composition than crystalline alloys[1–3]. However, the structure of amorphous alloys, which is in a sub-stable state in thermodynamics, will transform into crystalline structure at a certain temperature or long enough service time, i.e. crystallization will occur[4,5]. This structural transformation will affect various properties of amorphous alloys, such as mechanical and electrochemical properties, thereby affecting their practical applications[6–8]. On the one hand, the appearance of excessive crystalline phases in amorphous alloys will reduce their mechanical properties[9,10], on the other hand, the performances of amorphous alloys materials will be improved when there are nanocrystals with appropriate size in amorphous alloys[11].

In recent years, Zr-based bulk amorphous alloys have received extensive attention due to their excellent amorphous forming ability and excellent thermoplastic forming ability[12–15]. The improvement of thermoplastic processing performances by inhibiting the crack expansion and avoiding crystallization during thermoplastic processing of Zr-based bulk amorphous alloy[16,17], and sought to enhance the thermal stability of amorphous alloys by adding a small amount of rare earth elements to improve the product properties after thermoplastic processing[18,19]. The thermal stability, crystallization kinetics of amorphous alloys are related to thermoplastic forming ability and hot workability of bulk amorphous alloys[20–23]. Although there has been a lot of research work in this area, there are still many issues that are still unclear. In this paper, $Zr_{55.7}Cu_{22.4}Ni_{7.2}Al_{14.7}$ (at.%) alloy specimens were prepared by copper mold suction casting method. The isothermal crystallization kinetics was studied by X-ray diffraction (XRD) and differential scanning calorimetry (DSC), in order to further understand the crystallization mechanism, local Avrami exponent and crystallization activation energy of amorphous alloy. It will lay a theoretical foundation for thermoplastic processing and engineering application of bulk amorphous alloys.

[1]School of Materials and Energy, Guangdong University of Technology, Guangzhou 510006, People's Republic of China. [2]Guangdong Kiatest Technology Co., LTD, Guangzhou 510700, People's Republic of China. [3]Guangdong - Hong Kong Joint Research and Development Center On Advanced Manufacturing Technology for Light Alloys, Institute of New Materials, Guangdong Academy of Sciences, Guangzhou 510650, People's Republic of China. ✉email: pjtao@gdut.edu.cn
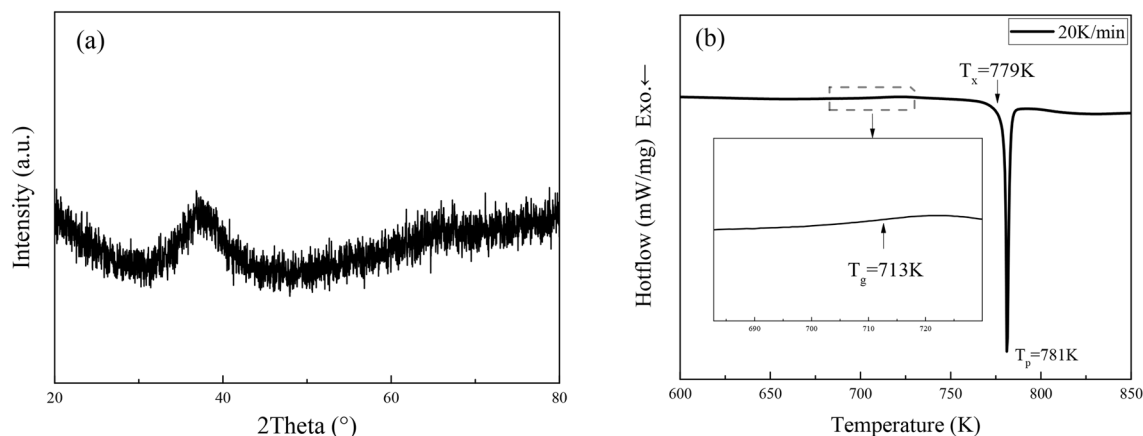
Figure 1. (**a**) XRD pattern and (**b**) DSC scan of $Zr_{55.7}Cu_{22.4}Ni_{7.2}Al_{14.7}$ alloy specimen.

Experimental

The ingots of $Zr_{55.7}Cu_{22.4}Ni_{7.2}Al_{14.7}$ (at.%) alloy were prepared under a Ti-gettered purified argon atmosphere in a WK-II non-consumable vacuum arc melting furnace using a mixture of high purity metals consisting of Zr (99.96 wt.%), Cu (99.98 wt.%), Ni (99.9 wt.%) and Al (99.97 wt.%). Each alloy ingot was re-melted at least four times for compositional homogeneity. Alloy ingots were re-melted and suction cast into water-cooled copper mold to obtain alloy robs with a diameter of 3 mm. The prepared specimens were characterized by XRD (D/MAX-Ultima IV, Cu-K_α radiation) with a wavelength (λ) of 1.54056 Å, and DSC (204 F1) in a high purity argon atmosphere. The specimen was heated from room temperature to 873 K at a heating rate of 20 K/min to determine its thermodynamic parameters. The isothermal crystallization kinetic parameters were obtained by heating to a series of temperature points (723 K, 733 K, 743 K, 748 K, 753 K, and 758 K) during supercooled liquid region (SLR) under a heating rate of 120 K/min and then held for an hour using DSC Q2000. The isothermal crystallization behavior and crystallization activation energy of the alloy specimens were analyzed using the Johnson–Mehl–Avrami model and the Arrhenius equation to obtain an evaluation of the thermal stability of amorphous alloy.

The functional relationship between the crystallization volume fraction $x(t)$ and the time t in isothermal crystallization process can be expressed by the Johnson–Mehl–Avrami (JMA)[24] equation: $x(t) = 1 - exp\{-[k(t-\tau)]^n\}$. Where $k = k_0 exp(-E/RT)$ is the reaction rate constant, E is the activation energy, k_0 is the constant, R is the molar gas constant, τ is the incubation time, and n is the Avrami exponent (which can reflect the crystallization mechanism of nucleation and nucleus growth during the crystallization process). The logarithm of both sides of the JMA equation can be obtained as follows[12]: $ln\{-ln[1-x(t)]\} = n\,lnk + n\,ln(t-\tau)$.

Results and discussion

Identification of alloy specimen structure.
Figure 1a shows XRD pattern of the prepared $Zr_{55.7}Cu_{22.4}Ni_{7.2}Al_{14.7}$ alloy specimen. It can be seen that the diffraction angle (2 theta) is between 32° and 42°, and there is a diffuse scattering peak without sharp crystal diffraction peak, which indicates that the structure of the alloy specimen is amorphous.

Characteristic temperature of $Zr_{55.7}Cu_{22.4}Ni_{7.2}Al_{14.7}$ bulk amorphous alloy.
The DSC scan curve of $Zr_{55.7}Cu_{22.4}Ni_{7.2}Al_{14.7}$ bulk amorphous alloy specimen at a heating rate of 20 K/min is shown in Fig. 1b. The curve shows a single exothermic peak, which is the exothermic reaction of the specimen after the supercooled liquid region (SLR). The glass transition temperature (T_g) of this amorphous alloy is 713 K, the onset of crystallization temperature (T_x) is 779 K, the crystallization peak temperature (T_p) is 781 K, and the SLR is $\Delta T = T_x - T_g = 66$ K. It indicates that the bulk amorphous alloy has a wide SLR, which is extremely beneficial to thermoplastic processing[8].

Kinetic analysis of isothermal crystallization.
The DSC curves of isothermal crystallization measurements of alloy specimens at 723 K, 733 K, 743 K, 748 K, 753 K, and 758 K, respectively, are shown in Fig. 2a at the top. Except for the test curve at 723 K, each curve shows a complete exothermic peak, and the appearance time of the crystallization peak decreases with increasing temperature, and the width of the crystallization peak becomes narrower and gradually sharp. The result expresses that heating at a constant temperature above 723 K for an hour, the time required for the alloy specimen to complete the crystalline transformation shortens as the holding temperature rises. XRD patterns of the specimens after annealing at the given temperatures are shown in Fig. 2b. All specimens exhibit obvious crystal diffraction peaks of crystallized phase after annealing at the given temperatures, but the intensity of diffraction peaks is lower for the specimen annealed at 723 K. It indicates that all the alloy specimens have been fully crystallized within the annealing time, except for the specimen annealed at 723 K where partial crystallization occurred. It is consistent with the analytical results of isothermal crystallization DSC.
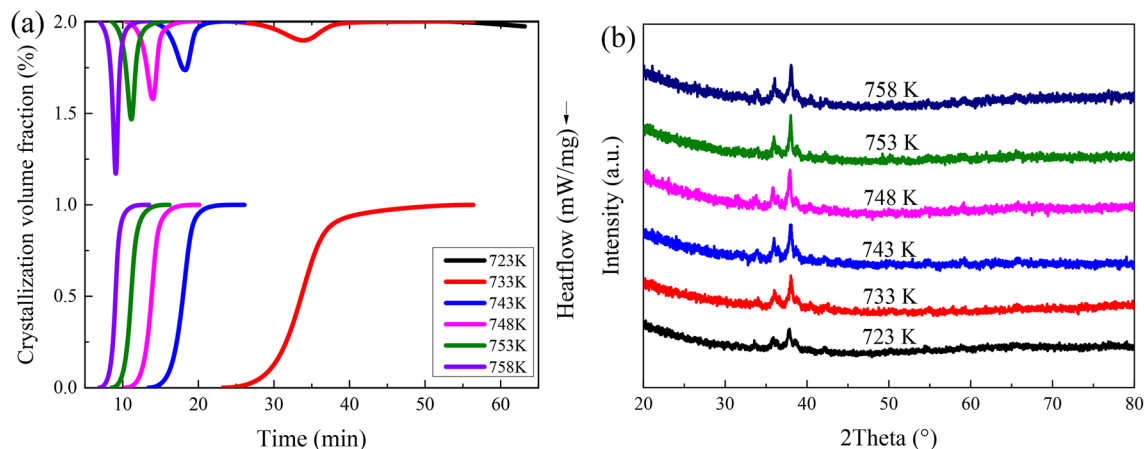
Figure 2. (**a**) Isothermal DSC scans at the top and the crystallization volume fraction at the bottom, (**b**) XRD patterns of the specimens after annealing at the given temperatures.
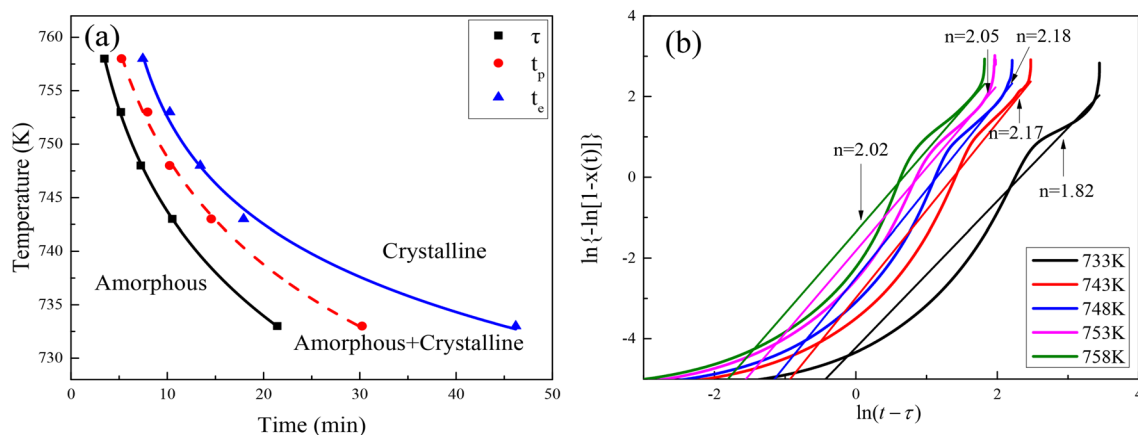

Figure 3. (**a**) Isothermal TTT curves and (**b**) JMA curves at different temperatures.

The heating time t and isothermal crystallization volume fraction $x(t)$ can be calculated by $x(t) = [\int_{t_0}^{t}(dH_c/dt)dt]/[\int_{t_0}^{t\infty}(dH_c/dt)dt] = A_t/A_\infty$[12,18,25]. Where A_t denotes the area of the exothermic peak between the onset of crystallization time t_0 and time t, H_c is the value of time t corresponding to the heat flow, and A_∞ denotes the total area of the crystallization exothermic peak.

The relationship between the crystallization volume fraction x and time t for $Zr_{55.7}Cu_{22.4}Ni_{7.2}Al_{14.7}$ bulk amorphous alloy at different temperatures is presented in Fig. 2a at the bottom. All the curves show S-shape (sigmoidal) with the increasing annealing time, and the S-shape becomes steeper and steeper as the temperature increases, implying that the crystallization rates are increased sharply with the increase of annealing temperature. In the initial stage of crystallization, the crystallization rate is slow, due to crystal nucleation takes a long time to break through the energy barrier. Subsequently, the crystallization rate is extremely fast, because a large number of nuclei are accumulated inside the specimen in the initial stage of crystallization and the nuclei grow rapidly by subsequently, and the volume content of crystals inside the specimen rises suddenly. At the end of crystallization, the nucleation rate drops quickly with the annealing time increases. The amorphous sample structure is almost transformed into a crystalline structure[20,26,27].

Figure 3a shows the Time–Temperature-Transformation (TTT) fitting curves[19,28] of the alloy specimens. Start, 50% fraction and end of crystallization phase transformations correspond to the crystallization incubation time τ, the peak crystallization time t_p, and the end of crystallization time t_e, respectively. At the bottom left of the curve is the amorphous region, where crystallization of amorphous alloy begins after crossing the onset of crystallization transition curve, and at the top right is the crystalline region where crystallization has been completed. As the annealing temperature increases, the crystallization incubation time τ is gradually reduced, and the time required for the specimen to complete crystallization is also significantly shortened. This is because atoms can get more energy to accelerate the fluctuation of internal atomic concentration at higher annealing temperatures, making the atomic motion more active and increasing the atomic mobility, which leads to rapid crystallization of the internal structure of bulk amorphous alloy[19].

As shown in Fig. 3b, the JMA curves of the specimens at different temperatures are obtained by plotting $ln\{-ln[1-x(t)]\}$ versus $ln(t-\tau)$. A linear fit to the JMA curve yields the slope and intercept of the line, with the slope corresponding to the Avrami exponent n and the intercept to the reaction rate constant k. The Avrami
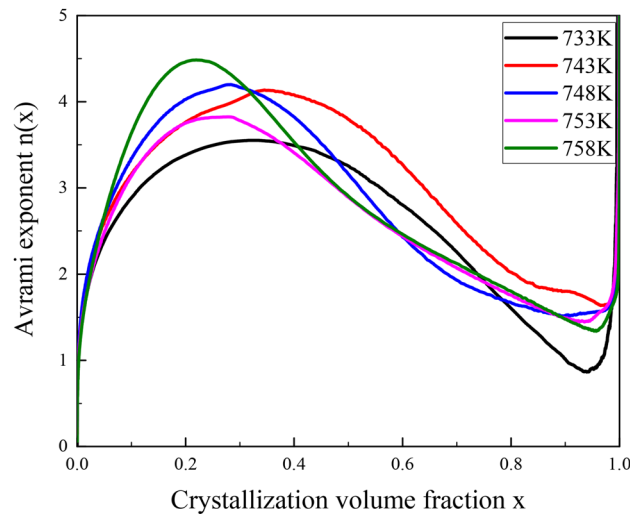
**Figure 4.** Curves between local Avrami exponent and crystallization volume fraction.

exponent values are distributed between 1.8 and 2.2, indicating that the crystallization mechanism is similar at different temperatures[29]. The reaction rate constant k increases with rising temperature, revealing that the alloy is easier to crystallize at higher temperatures, due to the fact that the diffusion ability of internal atoms increases with rising temperature, and the diffusion of atoms facilitates structural ordering, so the crystallization reaction rate of bulk amorphous alloy increases with rising temperature[20].

The crystallization behavior of amorphous alloys will show a certain variation pattern with the change of crystallization volume fraction x. During the crystallization of amorphous alloys, metastable phases may appear, and will transform into stable phases or transform into other sub-stable phases first and subsequently transform into stable phases[23,27]. Hence, Calka[30] proposed that the mechanism of nucleation and growth behavior can be characterized in more detail by analyzing the variation pattern of the local Avrami exponent. The local Avrami exponent $n(x)$ can be expressed by the expression: $n(x) = \{\partial ln[-ln(1-x)]/\partial ln(t-\tau)\}$. Ranganthan proposed that the local Avrami exponent n can be expressed by the formula[31,32]: $n = a + bp$. Where a is the nucleation mechanism parameter; b is the dimension of crystal nucleus growth; p is the growth mechanism parameter. And a, b and p content the following definitions: $a = 0$ indicates that the nucleation rate is zero; $a = 1$ indicates that the nucleation rate is constant; $a > 1$ indicates that the nucleation rate increases with time; $a < 1$ indicates that the nucleation rate decreases with time. $b = 1, 2, 3$ respectively represent one-dimensional, two-dimensional, and three-dimensional growth. $p = 0.5$ indicates the growth of diffusion-controlled; $p = 1.0$ indicates the growth of interface-controlled[20].

Figure 4 shows the relationship curves between the local Avrami exponent $n(x)$ and the crystallization volume fraction x of the alloy. Each curve has a similar trend with respect to the crystallization volume fraction x, indicating that the $n(x)$ does not vary much under the influence of different temperatures. At the same temperature, $n(x)$ varies significantly with x increasing, which exposes that the crystallization mechanism of bulk amorphous alloy is different at different crystallization stages[20].

The crystallization behavior of $Zr_{55.7}Cu_{22.4}Ni_{7.2}Al_{14.7}$ alloy specimen at a temperature of 758 K is analyzed as follows: the Avrami exponent n increases with the crystallization volume fraction to 4.5 and drops sharply to 1.5 by subsequently, indicating that the nucleation behavior of the crystal phase in this alloy is first interface-controlled and then transform to a diffusion-controlled growth behavior[20,23]. In the initial stage of crystallization, the value of n is quite tiny, indicating that nucleation rate is pretty slow, because there are a large number of supercooled liquid without nucleation in the specimen, and there are a large amount of short-range ordered atomic clusters, which assume the role of supercritical nuclei to discourage the formation of new crystal nuclei[28]. When $10\% < x < 37\%$, n rises to 4.5 and then reduces to 4, indicating that the alloy crystallization nucleation rate is accelerated with the increase of x. The crystallization behavior is controlled by the interface-controlled three-dimensional growth mechanism. This is because the previous nucleation growth in amorphous alloy will cause the composition change of the surrounding matrix[12]. Thus, it promotes the formation of new nuclei. When $37\% < x < 50\%$, n decreases from 4 to 3, indicating that the crystallization nucleation rate decreases with x. Its nucleation growth behavior is still controlled by interface-controlled, and both supercritical nuclei and new nuclei generated demand for undergoing atomic rearrangement, however, the tight and irregular structure of atomic arrangement of multi-component bulk amorphous alloy makes atomic diffusion difficult[28], which blocks the generation of new crystal nuclei. When $50\% < x < 95\%$, n reduces to 1.5, indicating that the nucleation growth dominates in this stage and the nucleation growth behavior transforms to diffusion-controlled[20]. That is why the internal crystallization nucleation rate decreases. When $x > 95\%$, the data at this stage will not be discussed on account of the large error of n value calculated by the JMA model. Therefore, heat treatment or thermal processing should be carried out at a lower temperature with SLR, while the heat treatment time should be reduced accordingly when the thermal processing temperature rises[8].

In addition to the Avrami exponent evaluation, the crystallization behavior of amorphous alloys can also be characterized by the change of crystallization activation energy. The activation energy of crystallization is
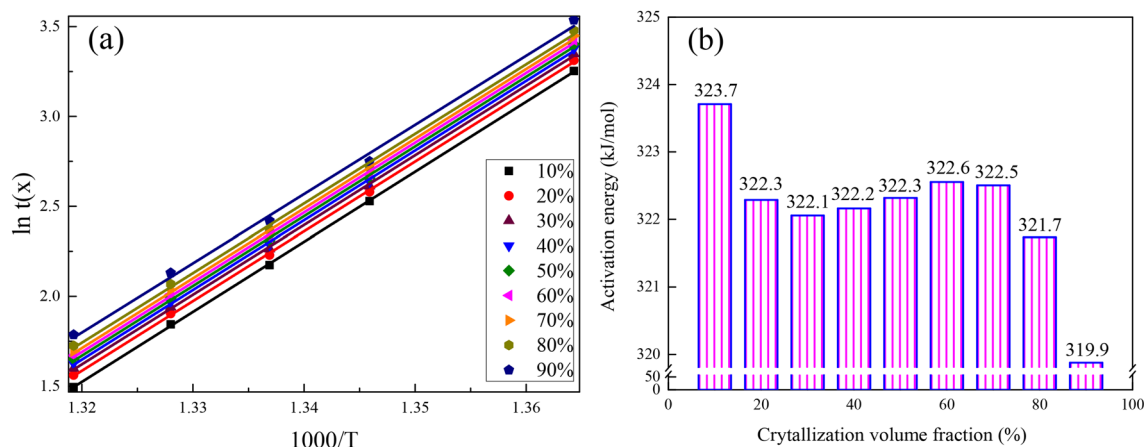
Figure 5. (**a**) Plots of *ln t*(*x*) versus 1000/*T* and (**b**) activation energy E_a versus crystallization volume fractions.

calculated by Arrhenius equation[12,33]: $t(x) = t_0 exp(E_a/RT)$. Where $t(x)$ is the time corresponding to crystallization volume fraction x, t_0 is a constant, E_a is the crystallization activation energy, R is the molar gas constant, and T is the corresponding isothermal crystallization temperature.

Figure 5a is obtained by plotting *ln t*(*x*) versus *1000/T* and linear fitting the data under each crystallization volume fraction. The slope obtained by linear fitting can be calculated by the Arrhenius equation to acquire the relationship curve between the crystallization activation energy and the crystallization volume fraction x[8], as shown in Fig. 5b. The crystallization activation energy of bulk amorphous alloy shows a decreasing trend as x increases. In the initial stage of crystallization, the higher activation energy of crystallization indicates that the alloy needs to break through a higher energy barrier for crystallization[20]. The crystallization activation energy decreases rapidly when $10\% < x < 20\%$, implying that the crystallization behavior becomes easier after the initiation of crystallization. When $20\% < x < 70\%$, the crystallization activation energy is basically stable at 322.3 kJ/mol, indicating that the crystallization reaction is comparatively stable in this process. When $x > 70\%$, the crystallization activation energy reduces rapidly, indicating that the new crystal nucleation rate reduces rapidly in the ultimate stage of crystallization, the crystallization behavior transforms into crystals growth, and the residual amorphous matrix volume content inside alloy gradually decreases[12]. Therefore, it is difficult for atoms in amorphous alloys to advance nucleation, and the structure of amorphous alloy becomes comparatively stable after crystallization behavior[34]. This is basically consistent with the analysis result of Fig. 4. The average crystallization activation energy of this bulk amorphous alloy is 322.1 kJ/mol, which is higher than the other components' in the same system of Zr–Cu–Ni–Al[12]. Thus, $Zr_{55.7}Cu_{22.4}Ni_{7.2}Al_{14.7}$ bulk amorphous alloy has relatively great thermal stability.

Conclusions

The structure of the prepared $Zr_{55.7}Cu_{22.4}Ni_{7.2}Al_{14.7}$ alloy specimen is amorphous. The glass transition temperature (T_g), the onset of crystallization temperature (T_x) and the crystallization peak temperature (T_p) are 713 K, 779 K, and 781 K, respectively, and the supercooled liquid region ($\triangle T = T_x - T_g$) is 66 K. The crystallization incubation times are shortened and the crystallization transformation rates increase with the rise of temperature. The Avrami exponents are situated at 1.8 ~ 2.2. As the crystallization volume fraction (x) increases, the crystallization nucleation rate shows a trend of first increasing and decreasing by subsequently, while the crystallization activation energy (E_a) decreases monotonously. The average crystallization activation energy is 322.1 kJ/mol, in the same time, the crystallization behavior transforms from interface-controlled to diffusion-controlled growth. The $Zr_{55.7}Cu_{22.4}Ni_{7.2}Al_{14.7}$ amorphous alloy has a great thermal stability.

References

1. Pang, D. X., Wang, J. T., Ding, B. Z., Song, Q. H. & Yang, Z. J. Relationships between quenching rates and properties in amorphous alloys. *Mater. Lett.* **5**(11), 439–441. https://doi.org/10.1016/0167-577X(87)90059-0 (1987).
2. Švec, P. & Duhaj, P. Growth of crystalline phase in amorphous alloys. *Mater. Sci. Eng. B* **6**(4), 265–271. https://doi.org/10.1016/0921-5107(90)90123-S (1990).
3. Wang, W. H., Dong, C. & Sheck, C. H. Bulk metallic glasses. *Mater. Sci. Eng. R* **44**(2–3), 45–89. https://doi.org/10.1016/S0966-9795(03)00046-3 (2004).
4. Inoue, A. Stabilization of metallic supercooled liquid and bulk amorphous alloys. *Acta Mater.* **48**, 279–306. https://doi.org/10.1016/S1359-6454(99)00300-6 (2000).
5. Peng, C. *et al.* Crystallization kinetics of $Zr_{60}Cu_{25}Fe_5Al_{10}$ bulk metallic glass. *J. Non-Cryst. Solids* **405**, 7–11. https://doi.org/10.1016/j.jnoncrysol.2014.08.030 (2014).
6. Johnson, W. L. *et al.* Beating crystallization in glass-forming metals by millisecond heating and processing. *Science* **332**(6031), 828–833. https://doi.org/10.1126/science.1201362 (2011).

7. Rahvard, M. M., Tamizifar, M. & Boutorabi, S. M. A. Non-isothermal crystallization kinetics and fragility of $Zr_{56}Co_{28}Al_{16}$ and $Zr_{56}Co_{22}Cu_6Al_{16}$ bulk metallic glasses. *J. Therm. Anal. Calorim.* **134**, 903–914. https://doi.org/10.1016/j.jnoncrysol.2017.10.026 (2018).
8. Błyskun, P., Latuch, J. & Kulik, T. Isothermal stability and selected mechanical properties of $Zr_{48}Cu_{36}Al_8Ag_8$ bulk metallic glass. *Arch. Metall. Mater.* **62**, 3. https://doi.org/10.1515/amm-2017-0266 (2017).
9. Yang, N., Yi, J., Yang, Y. H., Huang, B. & Wang, G. Temperature effect on fracture of a Zr-based bulk metallic glass. *Materials* **13**(10), 2391. https://doi.org/10.3390/ma13102391 (2020).
10. Song, K. K. *et al.* Correlation between glass-forming ability, thermal stability, and crystallization kinetics of Cu–Zr–Ag metallic glasses. *J. Appl. Phys.* **112**(6), 869. https://doi.org/10.1063/1.4752263 (2012).
11. Cai, J., Liu, H., Zhu, J. & Wang, Z. Effect of nanocrystalline process on microstructure of Zr-based metallic glass. *Mater. Res. Express* **6**(2), 11. https://doi.org/10.1088/2053-1591/aaf014 (2019).
12. Liu, L., Wu, Z. F. & Zhang, J. Crystallization kinetics of $Zr_{55}Cu_{30}Al_{10}Ni_5$ bulk amorphous alloy. *J. Alloy Compd.* **339**(1–2), 90–95. https://doi.org/10.1016/S0925-8388(01)01977-6 (2002).
13. Li, C. Y. *et al.* A thermal processing map of a ZrCuNiAlEr bulk metallic glass in the supercooled liquid region. *J. Mater. Sci.* **54**(9), 7246–7255. https://doi.org/10.1007/s10853-019-03363-5 (2019).
14. Kumar, G., Rector, D., Conner, R. D. & Schroers, J. Embrittlement of Zr-based bulk metallic glasses. *Acta Mater.* **57**(12), 3572–3583. https://doi.org/10.1016/j.actamat.2009.04.016 (2009).
15. Chen, Q. J. *et al.* A new criterion for evaluating the glass-forming ability of bulk metallic glasses. *Mater. Sci. Eng. A* **A433**, 155–160. https://doi.org/10.1016/j.msea.2006.06.053 (2006).
16. Zhang, Q. S., Zhang, H. F., Ding, B. Z. & Hu, Z. Q. Compressive fracture of $Zr_{55}Al_{10}Ni_5Cu_{30}$ bulk amorphous alloy at high temperatures. *Mater. Sci. Eng. A* **360**(1–2), 280–284. https://doi.org/10.1016/S0921-5093(03)00465-9 (2003).
17. Cheng, S. R., Wang, C. J., Ma, M. Z., Shan, D. B. & Gou, B. Mechanism for microstructural evolution induced by high temperature deformation in Zr-based bulk metallic glasses. *J. Alloys Compd.* **676**, 299–304. https://doi.org/10.1016/j.jallcom.2016.03.145 (2016).
18. Yang, K., Li, Y., Li, B., Li, J. & Fan, X. Effect of yttrium addition on the non-isothermal crystallization kinetics and fragility of Cu–Zr–Al bulk metallic glass. *Thermochim. Acta* **642**, 105–110. https://doi.org/10.1016/j.tca.2016.08.001 (2016).
19. Sikan, F., Polat, G., Kalay, I. & Kalay, Y. E. Effect of Sm on crystallization kinetics of Cu–Zr–Al metallic glasses. *Thermochim. Acta* **683**, 178439. https://doi.org/10.1016/j.tca.2019.178439 (2020).
20. Gao, Q. & Jian, Z. Y. Kinetics analysis of the isothermal crystallization of $Cu_{55}Zr_{45}$ metallic glass by differential scanning calorimetry. *Int. J. Chem. Kinet.* **51**(12), 903–908. https://doi.org/10.1002/kin.21318 (2019).
21. Lee, K. S., Ha, T. K., Ahn, S. & Chang, Y. W. High temperature deformation behavior of the $Zr_{41.2}Ti_{13.8}Cu_{12.5}Ni_{10}Be_{22.5}$ bulk metallic glass. *J. Non-Cryst. Solids* **317**(1–2), 193–199. https://doi.org/10.1016/S0022-3093(02)01998-1 (2003).
22. Chan, K. C., Liu, L. & Wang, J. F. Superplastic deformation of $Zr_{55}Cu_{30}Al_{10}Ni_5$ bulk metallic glass in the supercooled liquid region. *J. Non-Cryst. Solids* **353**(32), 3758–3763. https://doi.org/10.1016/j.jnoncrysol.2007.05.143 (2007).
23. Pauly, S., Das, J., Mattern, N., Kim, D. H. & Eckert, J. Phase formation and thermal stability in Cu–Zr–Ti(Al) metallic glasses. *Intermetallics* **17**(6), 453–462. https://doi.org/10.1016/j.intermet.2008.12.003 (2009).
24. Avrami, M. Granulation, phase change, and microstructure. *J. Chem. Phys.* **9**, 177–184. https://doi.org/10.1063/1.1750872 (1941).
25. Cui, J. *et al.* Crystallization kinetics of $Cu_{38}Zr_{46}Ag_8Al_8$ bulk metallic glass in different heating conditions. *J. Non-Cryst. Solids* **404**, 7–12. https://doi.org/10.1016/j.jnoncrysol.2014.07.029 (2014).
26. Wolny, J., Kokoszka, R., Sołtys, J. & Barta, P. Kinetics of crystallization of amorphous alloys under isothermal annealing-activation energy determination. *J. Non-Cryst. Solids* **113**, 171–177. https://doi.org/10.1016/0022-3093(89)90008-2 (1989).
27. Mandal, S., Lee, D. E. & Park, T. Crystallization kinetics of $Cu_{60}Zr_{25}Ti_{15}$ and $(Cu_{60}Zr_{25}Ti_{15})_{95}Ni_5$ bulk metallic glasses by differential scanning calorimetry (DSC). *J. Therm. Anal. Calorim.* **145**, 467–474. https://doi.org/10.1007/s10973-020-09735-3 (2020).
28. Rashidi, R., Malekan, M. & Gholamipour, R. Crystallization kinetics of $Cu_{47}Zr_{47}Al_6$ and $(Cu_{47}Zr_{47}Al_6)_{99}Sn_1$ bulk metallic glasses. *J. Non-Cryst. Solids* **498**, 272–280. https://doi.org/10.1016/j.jnoncrysol.2018.06.042 (2018).
29. Gao, Q. *et al.* Crystallization kinetics of the $Cu_{50}Zr_{50}$ metallic glass under isothermal conditions. *J. Solid State Chem.* **244**, 116–119. https://doi.org/10.1016/j.jssc.2016.09.023 (2016).
30. Calka, A. & Radliński, A. P. Decoupled bulk and surface crystallization in $Pd_{85}Si_{15}$ glassy metallic alloys: description of isothermal crystallization by a local value of the Avrami exponent. *J. Mater. Res.* **3**, 59–66. https://doi.org/10.1557/JMR.1988.0059 (1988).
31. Ranganathan, S. & Von Heimendahl, M. The three activation energies with isothermal transformations: applications to metallic glasses. *J. Mater. Sci.* **16**, 2401–2404. https://doi.org/10.1007/BF01113575 (1981).
32. Ramanan, V. R. & Fish, G. E. Crystallization kinetics in Fe–B–Si metallic glasses. *J. Appl. Phys.* **53**, 2273–2275. https://doi.org/10.1063/1.330797 (1982).
33. Wang, H. R. *et al.* Crystallization kinetics of an amorphous Zr–Cu–Ni alloy: calculation of the activation energy. *J. Alloys Compd.* **353**, 200–206. https://doi.org/10.1016/S0925-8388(02)01208-2 (2003).
34. Yang, Y. J. *et al.* Crystallization kinetics of a bulk amorphous Cu–Ti–Zr–Ni alloy investigated by differential scanning calorimetry. *J. Alloys Compd.* **415**, 106–110. https://doi.org/10.1016/j.jallcom.2005.07.062 (2006).

Acknowledgements

Author contributions

W.Z. and P.T. wrote the main manuscript text, Z.H. and K.Z. prepared Figs. 1 and 3, J.S. prepared Fig. 2, Y.C. prepared Figs. 4 and 5, and P.T. and Y.Y. provided language assistance. All authors reviewed the manuscript.

Competing interests

The authors declare no competing interests.

Additional information

Correspondence and requests for materials should be addressed to P.T.

Reprints and permissions information is available at www.nature.com/reprints.

Publisher's note Springer Nature remains neutral with regard to jurisdictional claims in published maps and institutional affiliations.